

THE OFFICIAL MAGAZINE OF THE OCEANOGRAPHY SOCIETY

# *Oceanography*

## CITATION

Simmons, H.L., and M.H. Alford. 2012. Simulating the long-range swell of internal waves generated by ocean storms. *Oceanography* 25(2):30–41, <http://dx.doi.org/10.5670/oceanog.2012.39>.

## DOI

<http://dx.doi.org/10.5670/oceanog.2012.39>

## COPYRIGHT

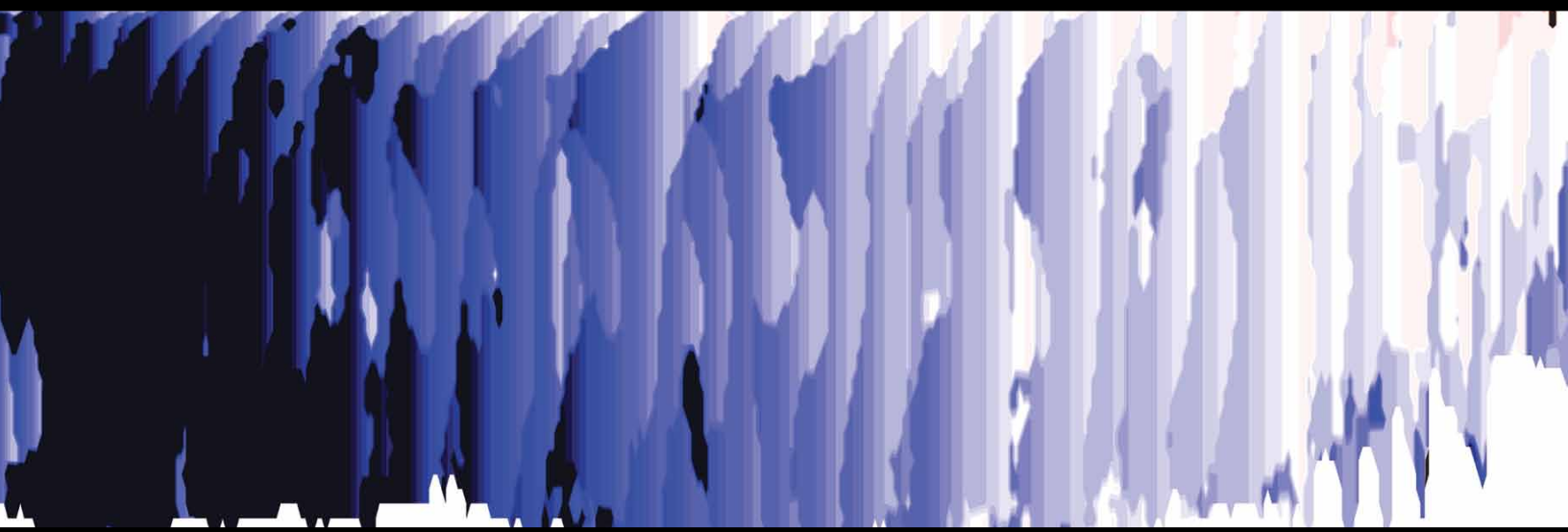
This article has been published in *Oceanography*, Volume 25, Number 2, a quarterly journal of The Oceanography Society. Copyright 2012 by The Oceanography Society. All rights reserved.

## USAGE

Permission is granted to copy this article for use in teaching and research. Republication, systematic reproduction, or collective redistribution of any portion of this article by photocopy machine, reposting, or other means is permitted only with the approval of The Oceanography Society. Send all correspondence to: [info@tos.org](mailto:info@tos.org) or The Oceanography Society, PO Box 1931, Rockville, MD 20849-1931, USA.

# Simulating the Long-Range Swell of Internal Waves Generated by Ocean Storms

BY HARPER L. SIMMONS AND MATTHEW H. ALFORD



**ABSTRACT.** Near-inertial waves (NIWs) are a special class of internal gravity waves with periods set by planetary rotation and latitude (e.g., at 30° latitude, one cycle per 24 hours). They are notable because they contain most of the observed shear in the ocean and around half the kinetic energy. As such, they have been demonstrated to mix the upper ocean and to have the potential to mix the deep ocean enough to be important for climate simulations. NIWs are principally generated as a result of a resonant coupling between upper-ocean currents and mid-latitude atmospheric cyclones. Here, we report on simulated NIWs in an eddy-resolving general circulation model that is forced by a realistic atmosphere, and we make comparisons to NIWs observed from moored and shipboard measurements of currents. The picture that emerges is that as much as 16% of NIW energy (which is season dependent) radiates out of the mixed layer and equatorward in the form of low-mode, long-lived internal gravity waves; they transmit energy thousands of kilometers from their regions of generation. The large amount of energy in near-inertial motions at a given site is a combination of a local response to wind forcing and waves that have traveled far from where they were generated.

## INTRODUCTION

### Motivation

Near-inertial waves (NIWs) are one of the most energetic modes of ocean variability, containing about half the ocean's kinetic energy at most sites (and even more beneath storm tracks). Hence, they are of central importance to a variety of ocean processes, including mixed-layer deepening (Price et al., 1986); submesoscale processes, larval dispersion, and formation of thin layers (Franks, 1995); restratification of mixed layers and thermohaline intrusions (Hosegood et al., 2008); and mixing of both the upper and deep ocean (Hebert

and Moum, 1994; Alford, 2003b). Yet, an understanding of NIW energy sources and redistribution by wave radiation is lacking, causing NIWs to be poorly represented in regional and global models.

Over the last decade, there has been significant community focus on internal tides, which produce large thermocline displacements, affect sound propagation, and control some hotspots of elevated turbulent mixing. Near-inertial internal gravity waves are probably of similar or greater importance, providing comparable kinetic energy and the vast majority of shear variance (Alford and Whitmont, 2007; Toole, 2007), and likely leading to a substantial amount of turbulent mixing. Significant deficiencies remain in our understanding of the physical processes that determine their generation, evolution, and destruction. NIWs appear to be primarily forced by the wind (D'Asaro, 1985; Alford and Whitmont, 2007). The amount of energy input to the ocean in the form of NIWs has been estimated to be 0.5–0.7 TW (Watanabe and Hibiya, 2002; Alford, 2003a), based on forcing a slab model (Pollard and Millard, 1970) with reanalysis winds. However, Jiang et al. (2005) demonstrated sensitivity to the choice of wind product used, obtaining values ranging from 0.36–1.4 TW. Though uncertain, these calculations represent a large fraction of the 2 TW of energy demand required to maintain deep-ocean stratification (Munk and Wunsch, 1998; Wunsch and Ferrari, 2004; St. Laurent and Simmons, 2006).

These calculations give the “source” of NIWs, specifically, the lateral distribution of the power input. However, analogous to internal tides, NIWs appear to be able to travel far from their forcing regions—downward into the ocean interior from their generation at the surface and also

equatorward. Understanding their dissipation clearly requires understanding this lateral and vertical propagation. In a study using a global model similar to the one used here, Furuichi et al. (2008) obtained a global wind work total of 0.35 TW, but without mesoscale flows. Though they obtained good agreement with some observational estimates of inertial energy in the mixed layer, they concluded that most NIW energy dissipates in the upper 150 m of the ocean. On the other hand, data from the Ocean Storms Experiment (D'Asaro, 1995; Levine and Zervakis, 1995) and historical moored current meters (Alford, 2003a) suggest that a substantial portion of NIW

energy is radiated far from generation regions in fast-moving, low-mode waves. Additionally, observations show energetic NIWs at all depths (Silverthorne and Toole, 2006; Alford, 2010), with a greater percentage penetrating to depth (Alford et al., in press) than concluded by the Furuichi study. One possibility for these discrepancies is that mesoscale flows can affect generation (Weller, 1982), refract the waves once generated (Kunze, 1986), and amplify deep propagation (Lee and Niiler, 1998; Zhai et al., 2005).

Our study, unlike the Furuichi simulation, includes mesoscale eddies (Figure 1). It is intended to shed some light on these puzzles, and illustrate the

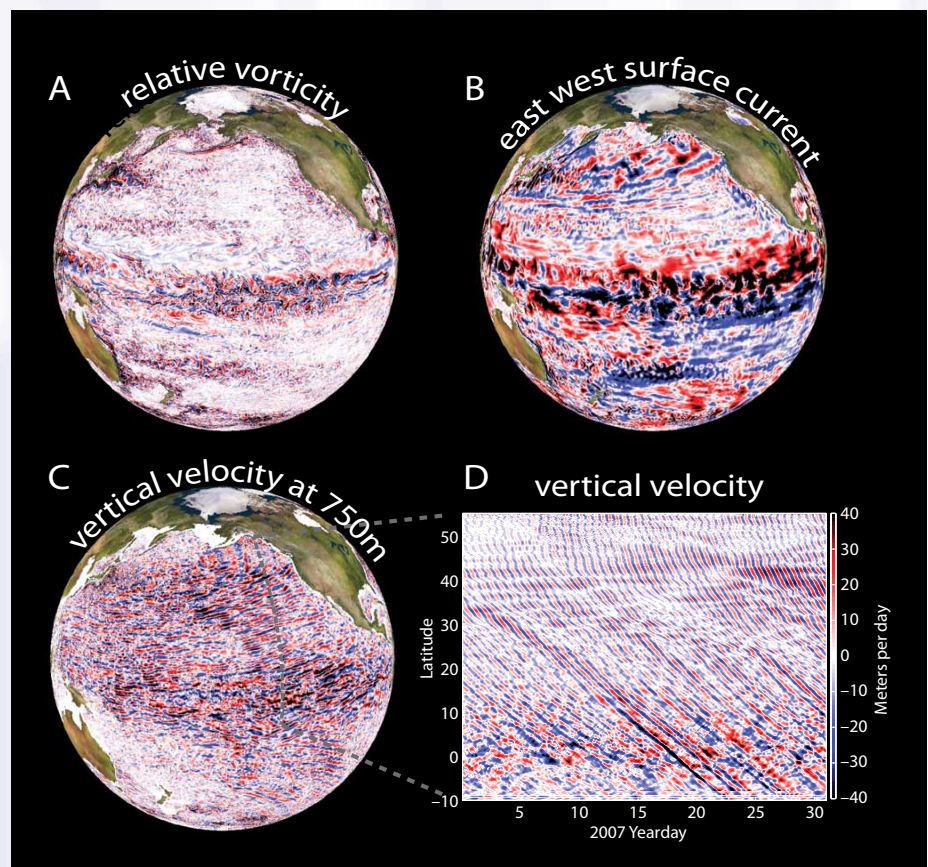


Figure 1. (A) Relative vorticity of sea surface currents, scaled by the Coriolis frequency at 30°N. Colormap saturates at 0.1. (B) Snapshot of east-west sea surface currents. Colormap saturates at 25  $\text{cm s}^{-1}$ . (C) Vertical velocity at 750 m depth. Colormap saturates at 40 m per day. (D) Time-latitude plot of vertical velocity at 750 m depth along the meridian indicated in (C). The data visualized in panels B–D have not been filtered or band passed in any way.



long-range-propagation aspects of the wave field in a fully eddying ocean. We find that from 3% to 16% of the energy radiates away in our model, depending on the season and the storm strength. Though the exact percentage is likely sensitive to details of the model and requires further study, we focus on the spatial structure of the radiated portion here to learn more about these long-propagating waves. Because we obtain many of the same results as the Furuichi study, the implication is that mesoscale flows affect the long-propagating waves only a little. However, they do likely affect the radiated versus local portion of the NIW wake of individual storms.

### Wind Generation of Near-Inertial Waves

The first part of NIW generation, the initial input of energy into the mixed layer by resonant forcing, is the best understood. Observed mixed-layer

velocities quickly grow as great as  $1 \text{ m s}^{-1}$  (greater in hurricanes and typhoons). A slab model by Pollard and Millard (1970) generally reproduces the initial amplitude and phase of observed mixed-layer oscillations. The skill of the slab model enables construction of the aforementioned global maps of wind work, using only reanalysis wind products such as those from the National Centers for Environmental Prediction (NCEP) and mixed-layer depth climatology. Note that recent work using high-resolution moored observations (Plueddemann and Farrar, 2006) pointed out that neglect of mixed-layer deepening by slab models likely causes these estimates to be high, although the degree of overestimation is uncertain and likely varies from place to place (Tom Farrar, Woods Hole Oceanographic Institution, *pers. comm.*, 2012). Slab models predict strong inputs in the western portion of each basin at mid-latitudes, confirming

that mid-latitude storms provide the bulk of the energy flux (with much of the remainder from hurricanes/typhoons). The general distribution of energy flux in our model (Figure 2, gray scale) resembles the observed near-inertial energy in the mixed layer from previous slab-model estimates and the observed distribution from drifters (Chaigneau et al., 2008), but the global total of 0.4 TW, as we will show, is on the low side of the range of estimates.

### Excitation of Interior Motions

Once near-inertial motions in the mixed layer are generated, lateral variation leads to convergences and divergences that “pump” vertical motions at the base of the mixed layer, driving motions in the ocean interior (Figure 3). Anderson and Gill (1979) and Gill (1985) developed a modal formalism for describing this excitation of submixed-layer motions. Much like the vibration of a guitar string, waves in the stratified ocean take the form of standing vertical oscillations of horizontal currents (with corresponding vertical displacements of isopycnals), which are termed the dynamic “modes.” The lowest mode, or, by analogy, “harmonic,” of horizontal velocity corresponds to horizontal ocean currents that are uniform from top to bottom. This mode is commonly referred to as the “barotropic” mode or zeroth mode

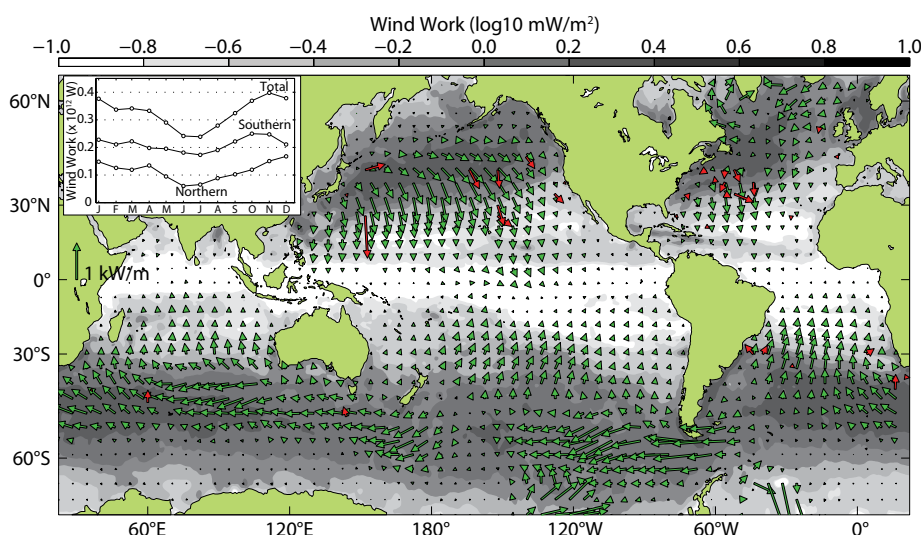


Figure 2. Model depth-integrated annual mean baroclinic energy flux (green arrows) and mooring-derived total near-inertial fluxes of Alford (2003b) (red arrows) over annual mean wind energy flux to near-inertial motions (gray scale). A  $1 \text{ kW m}^{-2}$  reference arrow is drawn over Africa. The model fluxes are smoothed over  $3^\circ \times 3^\circ$ , and every 24<sup>th</sup> gridpoint is plotted. The observed fluxes have been averaged together over bins when multiple moorings occur in a bin. The inset over Asia shows the wind work integrated over the global ocean (indicated as “Total”) and integrated over each hemisphere (northern and southern).

---

**Harper L. Simmons** ([hlsimmons@alaska.edu](mailto:hlsimmons@alaska.edu)) is Associate Professor of Marine Science, School of Fisheries and Ocean Sciences, University of Alaska Fairbanks, Fairbanks, AK, USA. **Matthew H. Alford** is Principal Oceanographer, Applied Physics Laboratory, and Associate Professor, School of Oceanography, University of Washington, Seattle, WA, USA.



and is not an internal gravity wave. The first “baroclinic” or depth-dependent mode, indicated schematically in gray in Figure 3, is an internal gravity wave that takes the form of an oscillation, with flow going in one direction at the surface and in the opposite direction at depth, and with a “node” at the depth of the thermocline. Higher modes have higher numbers of nodes and hence a more complicated vertical structure. An important feature of internal gravity waves is that the horizontal rate of propagation, or the “phase” speed, associated with each given baroclinic mode decreases with increasing mode number. For typical ocean depths and stratification, the first baroclinic mode travels at about  $3 \text{ m s}^{-1}$  and the second at  $1.5 \text{ m s}^{-1}$  zeroth mode. The expected vertical structure of the modes can be computed from stratification alone, and profiles can be described by fitting the velocity profile to a linear combination of the modes.

To compute the ocean interior response, the slab velocity profile (motion in the mixed layer and none below) is projected onto the modes computed for pre-storm stratification. As the modes propagate away, energy travels downward into the ocean interior, with the details controlled by the phasing between the various modes (see Figure 3). Far from the storm site, successive modes will arrive in the order of their phase speed so that we can expect to see the first mode arrive first, followed by the second, and so forth.

The initial puzzle of Gill’s work was how energy evolved from the large lateral scales of the forcing to smaller scales, which transfer energy more rapidly. The initial atmospheric forcing of the mixed layer tends to occur over hundreds of kilometers, the typical scale

of mid-latitude storms. Internal waves that are imprinted with these horizontal scales propagate downward into the ocean very slowly (one-year timescales), as group velocity is inversely proportional to wavelength. Several processes act to decrease the scales of mixed-layer motion coherence, allowing generation of waves with shorter horizontal wavelengths that can propagate downward into the stratified interior. The dominant process is the variation of inertial frequency with latitude, the so-called beta effect (D’Asaro, 1989). Mixed-layer motions at different latitudes oscillate at slightly different frequencies, so in the days following a storm passage, the meridional scale of coherence steadily shrinks to less than 100 km. In the groundbreaking Ocean Storms Experiment, D’Asaro (1995) validated this dynamical explanation. In particular, the role of the beta effect in leading to the initial growth of horizontal gradients

was clearly demonstrated, leading to a qualitative agreement with the theory for low modes. However, Gill’s formalism could not reproduce an observed “beam,” wherein energy migrated downward in time away from the mixed layer following storm events (see Figure 5 for recent evidence of downward-propagating energy).

While the beta effect is the most important process in generating the smaller scales that can propagate, the variability in the ocean response for similar wind events at station Papa in the North Pacific ( $50^\circ\text{N}$ ,  $145^\circ\text{W}$ ; Alford et al., in press) clearly implicates a role for other processes. Weller (1982) suggested that mesoscale eddies modify the near-inertial response in the mixed layer. Recent theoretical and numerical work has given still more credibility to the notion. The vorticity associated with energetic eddies can create an effective inertial frequency (the combination of

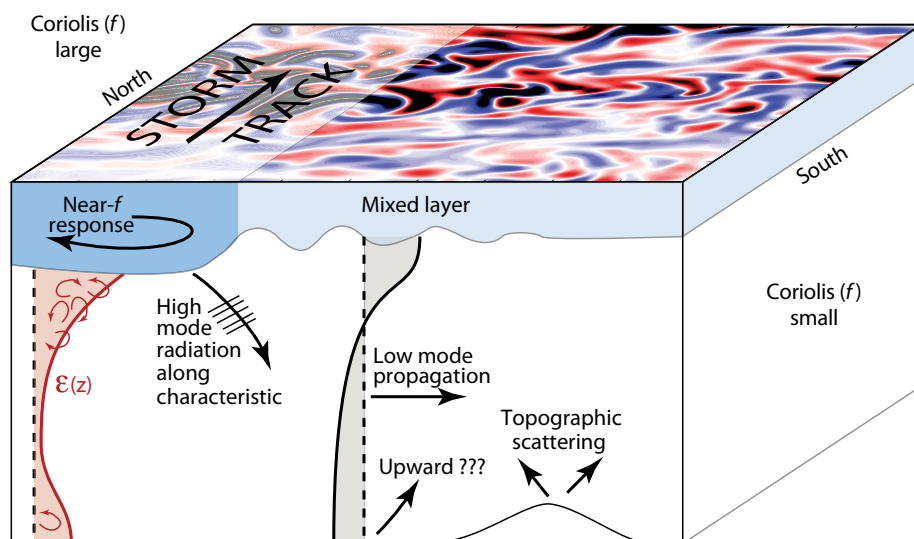


Figure 3. Processes associated with near-inertial generation, dissipation, and propagation. As storms move along the storm track, a local response occurs with frequencies near the local Coriolis frequency. Both high- and low-mode internal gravity waves are excited. High modes propagate along curving characteristics downward and equatorward. The higher modes have strong shear that results in mixing (“ $\epsilon$ ”). Low-mode wave radiation, indicated in gray, takes the form of oscillations that propagate equatorward. Upward characteristics and topographic scattering have been observed, but the processes involved are not completely understood.

relative and planetary vorticity; Kunze, 1985). Hence, in addition to “imprinting” mesoscales and submesoscales on NIWs (effectively reducing their wavelengths and increasing their propagation speeds), anticyclonic eddies can create regions known as “inertial chimneys” wherein a locally lowered effective inertial frequency allows rapid deep propagation. First proposed by Lee and Niiler (1998), inertial chimneys are also seen in numerical models (Zhai et al., 2005).

#### Local Dissipation vs. Long-Range Propagation

NIW evolution depends on vertical and horizontal wavelengths imparted onto interior motions by storms. The initial forcing excites all vertical modes in a red spectrum, with most energy going to the lowest modes. Horizontal scales are set through a combination of storm size and storm translation speed, plus the mesoscale vorticity field. Fundamental to understanding the energy cascade is determining the relative importance of (1) low-mode motions, which contain appreciable energy but quickly propagate away laterally, and (2) higher modes that remain in the forcing region owing to their slow vertical and meridional group velocities, and contain much of the vertical shear in the ocean. The distribution of the dissipation from a storm thus depends on the relative fraction of energy in each mode. Depending on the stratification, 30% or more of the energy may be contained in vertical modes one and two (D’Asaro, 1995; Alford, 2010; Alford et al., in press). These low-mode disturbances propagate horizontally out of the generation region and may break as a result of topographic scattering, as do internal tides (Müller and Liu, 2000; Johnston and Merrifield, 2003), or

nonlinear transfers within the internal wave field. The remainder of the energy is in higher wavenumber waves that have slow group velocities and greater shear, and are therefore likely to break relatively locally. The former are the focus of our study, in large part because our numerical model only resolves the first few vertical modes.

#### Blue Shift of the Ocean Current Spectrum Near the Inertial Frequency

Near-inertial waves are special for a few reasons (Garrett, 2001), most notably for our purposes because of their nearness to the lower end of the range of possible frequencies for propagating internal gravity waves, which can only exist between  $f$  (the local Coriolis frequency) and  $N$  (the buoyancy frequency). For this reason, near-inertial waves can only propagate slightly toward the pole on a beta plane, because they quickly reach a latitude where their frequency is equal to the local value of  $f$ , which is higher than their generation latitude, and then turn they toward the equator. Alford (2003b) first observationally demonstrated this tendency to propagate toward the equator. Note that this view contrasts with the original explanation of the near-inertial peak by Fu (1980) in terms of higher-frequency waves propagating *poleward*.

As a group of NIWs propagates down from the surface and toward the equator, it maintains the frequency associated with its generation latitude, which will exceed the local value of  $f$ . This phenomenon is commonly referred to as a blue shift, but it really arises from the reduction of  $f$  with latitude rather than an increase in the wave frequency. The terms “red” and “blue” refer to relatively lower and higher frequencies, analogous

to the relative frequencies of red and blue visible light. The consequence is that at any given latitude and depth, the internal gravity wave spectrum (as measured by, for instance, horizontal velocity) will have a locally generated peak near  $f$  plus a higher-frequency (bluer) contribution by waves that originated shallower than and poleward of the given location where  $f$  was higher. The blue shift can be quantified by a ratio of the local Coriolis frequency  $f$  to the near-inertial peak so that an  $f_{\text{peak}}/f_{\text{local}}$  larger than one represents a blue shift and, conversely, a ratio smaller than one reveals a “red” shift. A blue shift of the near-inertial peak has been reported throughout the world ocean (e.g., Fu, 1981; D’Asaro and Perkins, 1984).

#### MODEL DESCRIPTION

For this study, we used the Generalized Ocean Layer Dynamics (GOLD) model, an isopycnal-coordinate ocean model developed at the National Oceanic and Atmospheric Administration Geophysical Fluid Dynamics Laboratory. It is an evolution of the Hallberg Isopycnal Coordinate Model (HIM; Hallberg, 1997). Previously, HIM has been used to study global surface tides (Arbic et al., 2004) and baroclinic tides (Simmons et al., 2004a, 2011; Simmons, 2008).

Topography data were taken from the thirtieth-degree resolution ETOPO2 dataset (National Geophysical Data Center), bicubically interpolated to the target model grid resolution. Horizontal resolution is nominally one-eighth degree globally with resolution scaling from approximately  $14 \times 14$  km at the equator to  $7 \times 7$  km at  $60^\circ\text{N}$  (quasi-Mercator), transitioning to a quasi-regular bipolar grid (Murray, 1996)

poleward of 60°N where the resolution remains a nearly constant  $7 \times 7$  km.

Isopycnal viscosity was set by two additive schemes. The first is a biharmonic scheme whereby a fixed parameter that has units of velocity set to  $0.05 \text{ m s}^{-1}$  is multiplied by the third power of the grid resolution. The second scheme is a Smagorinsky nonlinear eddy viscosity computed by multiplying a fixed parameter with units of velocity set to  $0.001 \text{ m s}^{-1}$  times the grid spacing. The model time stepping uses a mode-splitting scheme with a time step of 360 seconds and 7.5 seconds for the baroclinic and barotropic modes, respectively. The nondimensional quadratic bottom drag coefficient is 0.003. Diapycnal mixing was calculated using the shear-driven entrainment scheme of Jackson et al. (2008). The mixed layer is modeled using a refined bulk mixed layer (Hallberg, 2003) extension to the traditional Krauss-Turner scheme employed in most isopycnal coordinate models.

The model was forced with wind stress and buoyancy fluxes obtained from a modified version of the annual repeating Common Ocean-ice Reference Experiments (CORE) atmospheric forcing data (Griffies et al., 2009). Turbulent fluxes are calculated with a Monin-Obhukov boundary layer scheme (Griffies et al., 2009) using the atmospheric state and the evolving model ocean. The CORE atmospheric data have six-hourly variability for most atmospheric fields, obtained from the NCEP analysis. It repeats annually, with numerous corrections to address known biases and to balance the fluxes when integrated over the global ocean and over a year. Notably, our forcing differs from the CORE scheme described by Griffies et al. (2009) in one important regard:

atmospheric forcing is computed from the CORE fields (e.g., relative humidity, radiative fluxes, and surface air temperature) except that 10 m winds from the 2007 NOGAPS (Navy Operational Global Atmospheric Prediction System)

and colleagues). Because the transects took one to three inertial periods to conduct, a technique known as “inertial back rotation” was used to reference observations to an arbitrary common time by assuming that currents rotate at

“AS IS TYPICAL FOR A MODEL OF THIS RESOLUTION, ENERGETIC MESOSCALE CIRCULATION DEVELOPS ALONG WITH LARGE-SCALE GENERAL CIRCULATION.”

data (Rosmond et al., 2002) at one-half degree spatial resolution and three hourly temporal resolution are used instead of the CORE winds.

The ocean was spun up for five years. Beginning January 1 of the sixth year, an intensive data archiving period was initiated, with the full global three-dimensional model velocity and isopycnal depth fields stored every two hours for a year. We regard the high-frequency component of the solution as a hindcast of actual wave events from 2007 excited by the NOGAPS winds, acknowledging that NIWs are influenced by mesoscale eddies, which are not expected to be representative of 2007 in detail.

#### DATA DESCRIPTION

Model output is compared to two types of observational data—a shipboard transect of shear in the North Pacific, and a global dataset of about 80 moorings. These datasets emphasize the high- and low-mode portions of the near-inertial signals, respectively. The shipboard transect was collected with the Hydrographic Doppler Sonar System installed on R/V *Roger Revelle* (recent work of Andy Pickering, author Alford,

the inertial period. The moorings, which were originally collected by a vast variety of investigators over 30 years, were selected by Alford (2003b) because they offered sufficient resolution in the vertical to estimate energy and energy flux. Near-inertial motions were isolated via band-pass filtering.

#### RESULTS

As is typical for a model of this resolution, energetic mesoscale circulation develops along with large-scale general circulation. A three-day-average view of sea surface vorticity from the model reveals many well-known features of ocean circulation: western boundary currents, a strong equatorial countercurrent system perturbed by tropical instability waves, and mesoscale vorticity throughout the world ocean (Figure 1A). If we look at instantaneous snapshots of ocean currents (Figure 1B), there are a great many transient velocity fluctuations that correspond to surface wind stress, most clearly under the storm tracks, as well as high-frequency oscillations that are NIWs (see below). The NIWs that are the subject of this paper are the zonally banded features evident in Figure 1A–C.



## The Basin-Scale Wake of Near-Inertial Waves

Much as the splash from a rock thrown into a pond will organize itself into a wave train emanating from a region of disturbance, the initial forcing of NIWs under the storm track is transformed into a wave train radiating equatorward. Looking deeper in the ocean (Figure 1C, vertical velocity at 750 m depth) eliminates much of the confusion of the upper ocean, which is subject to direct forcing by the atmosphere. An alternate view is revealed by plotting the vertical velocity versus latitude and time (Figure 1D) along the slice shown in Figure 1C. Later, we present a spectral analysis of the signals, confirming their near-inertial properties.

Banded fronts of NIWs with near-zonal transbasin coherence are somewhat evident in the instantaneous surface currents shown in Figure 1B, but they

are revealed much more clearly in Figure 1C,D. The latitude-time slice in Figure 1D shows that these waves travel thousands of kilometers, apparently without disruption by the lower-frequency flows. For example, around yearday 17, a wave train originating at 40°N crosses through the equator into the Southern Hemisphere. It should be noted that these structures are also evident in the deep vertical velocity response in the simulations of Furiuchi et al. (2008, their Figure 2), and in Komori et al. (2008, their Figure 1). A “shadow” in the lee of the Hawaiian Islands is evident (Figure 4). Komori et al. (2008) also noted the shadowing behind the Hawaiian Islands. It should be stressed that Figure 1C,D has not been filtered or band passed in any way. The dominance of the near-inertial velocity signal emphasizes the fact that inertial motions have most of the ocean’s energy.

## Modal Wake

A high-pass filter suppresses much of the general circulation because its characteristic timescale is days to months, and it further emphasizes near-inertial fluctuations. The pattern of NIWs is not particularly sensitive to the choice of filter, but we choose one that passes frequencies higher than 1/72 hours using a sixth-order Butterworth filter, and retains inertial signals for all latitudes poleward of 10° of latitude. We fit the model’s high-passed velocity fields to the dynamical normal modes, calculated by the method of Lighthill (1969). We only examine the first three normal modes because higher vertical modes have smaller meridional wavelengths and, hence, would not be adequately resolved by the model’s horizontal grid. Spatial maps of the surface velocity signature associated with the three modes are plotted in the left panels of Figure 4, and time-latitude plots along the indicated meridian are shown on the right. Radiation can be seen for each mode propagating toward the equator, with the slope in latitude-time of the features corresponding to the expected speed for each mode and with north-south wavelengths that decrease with increasing mode number. The fronts become increasingly zonal with increasing mode.

## Vertical Structure

A qualitative measure of the model’s ability to resolve the signals is seen by comparing the simulated vertical shear of horizontal velocity along a line north of Hawaii (upper panel, Figure 5) with observations (lower panel) from the transect collected by A. Pickering, author Alford, and colleagues on R/V *Roger Revelle* mentioned earlier. Propagation is along

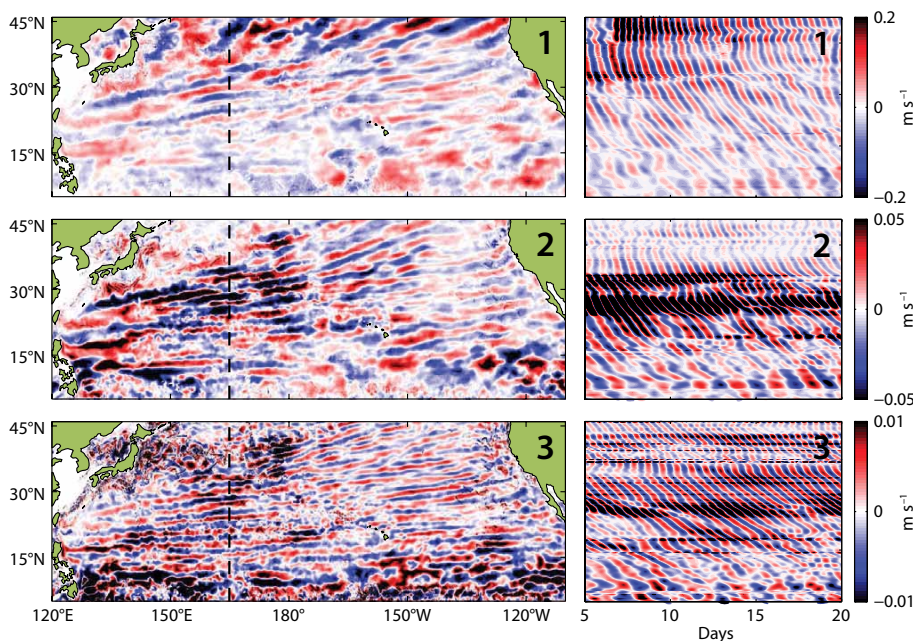


Figure 4. Left panels: Snapshots of the basin-scale wave wake for baroclinic modes 1–3, as indicated by the east-west surface currents associated with each mode. The number in the upper right of each panel indicates mode number. Right panels: latitude-time plot along the meridian indicated in the left panels.

“characteristics” (lines of characteristic slope), consistent with a frequency somewhat above  $f$ . Though collected in a different year, the general tendency to propagate downward and equatorward is seen in both model and observations. However, the observed shear is much greater, highlighting the model’s limited ability to resolve the higher modes. A characteristic is drawn for a frequency (i.e., a 3% blue shift; Garrett, 2001).

#### Latitudinal Propagation and Conservation of Frequency: Blue Shifting

We examine the frequency response of the model in several ways. We compute horizontal velocity spectra every half-degree in latitude and every 2° in longitude, and average at each latitude to produce maps of spectral power as a function of frequency and latitude for the North Pacific. The resulting spectra of the modal, surface, and deep currents (Figure 6) reveal strong inertial peaks. As internal waves propagate equatorward, they preserve their frequencies, which smear the spectra equatorward, as shown in the first three panels of

Figure 6. The fourth panel shows the effect of this “painting” of frequency equatorward: the inertial peaks, which are combinations of local inertial response and “contamination” from signals that originated at higher latitudes where  $f$  is larger, has been blue-shifted to higher frequency. In the example given

here, the shift is between 5 and 10% at 35°N for modes 1–4. The spectrum of the surface currents (green line) is narrower and less shifted, suggesting that the full sea surface current response is less contaminated by the long-range swell of NIWs arriving from higher latitudes. Conversely, the deep currents

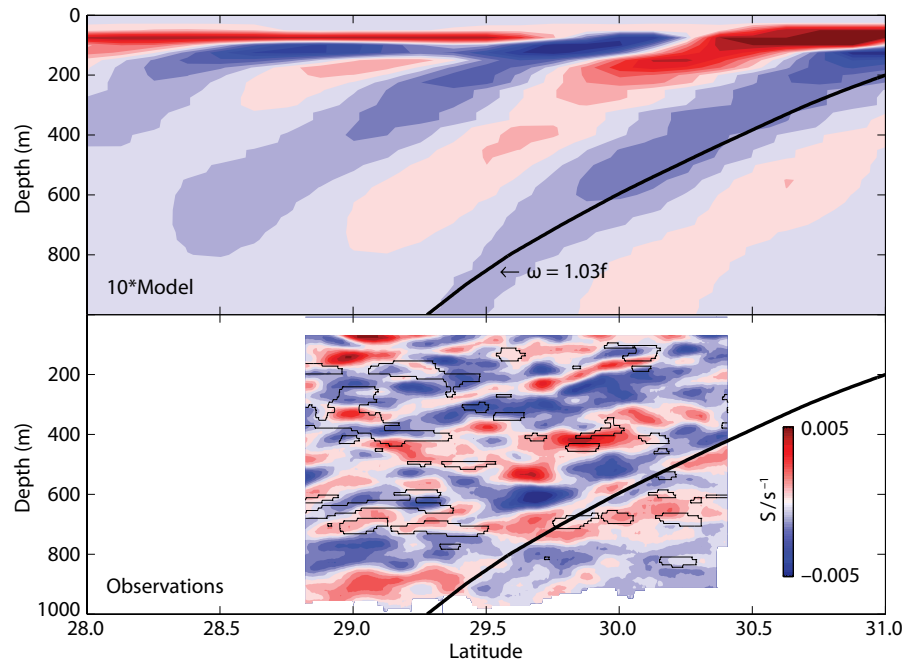


Figure 5. (top) Model shear in a section north of Hawaii. (bottom) R/V Roger Revelle sonar shear along the same section, inertially back rotated.

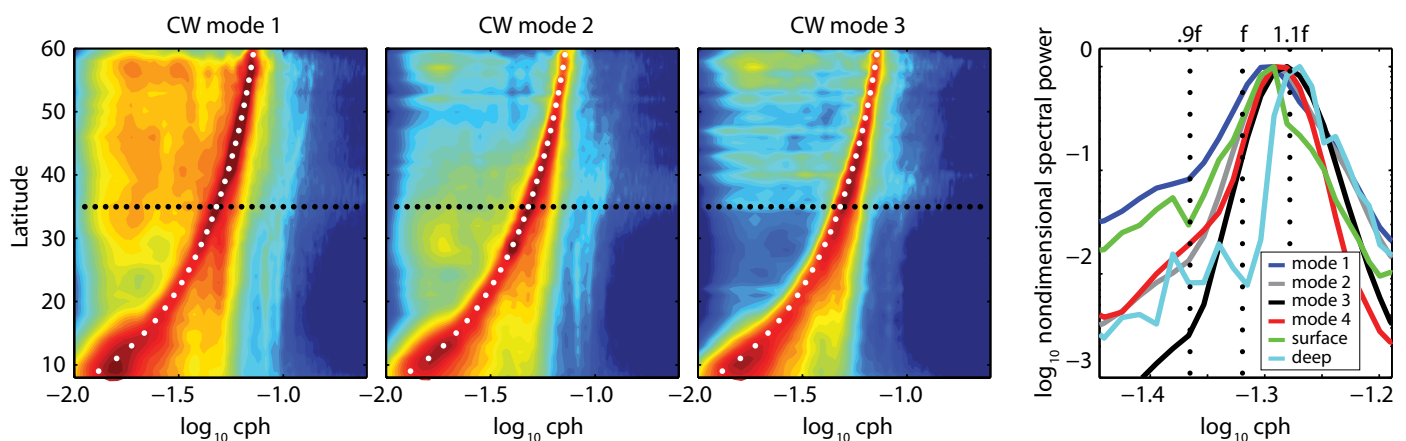


Figure 6. First three panels: spectral energy of modally analyzed clockwise currents (logarithmic color scale, arbitrary units) as a function of latitude and frequency for modes 1–3. White dots in the first three panels indicate the Coriolis (inertial) frequency at each latitude. The rightmost panel shows the near-inertial spectral power at 35°N (scaled to have a peak magnitude of 1 for each spectrum). All spectra are averages of spectra along meridians separated by 2° in the North Pacific.

experience a stronger blue shift.

The blue shifts of the full model currents were computed over a range of depths and latitudes in the North Pacific and also compared to mooring estimates of the blue shift (Figure 7). We see that the model and moorings have comparable blue shifts with latitude and depth from 25–60° latitude, with a small tendency for a weak red shift in the upper ocean. The model shows a very strong blue shift equatorward of 25°, but, unfortunately, there are so few reliable estimates from observations that no comparison can be made.

## Energetics

### Depth-Integrated Baroclinic Energy Flux

Energy flux was computed from the high-pass-filtered density and baroclinic velocity fields (Althaus et al., 2003; Simmons et al., 2004a). In the annual mean, NIWs propagate equatorward from Northern Hemisphere storm tracks, directed to the southeast, as shown in Figure 2. We have overlain the total mooring fluxes from Alford

(2003a). It should be noted that the comparison is imperfect because the model computed fluxes are averages from a simulation using 2007 winds, whereas Alford's estimates are a synthesis of different mooring deployments over many different years. Particularly in the North Pacific, the magnitude and direction of the model and mooring-derived estimates of the low-mode flux are in agreement. In the Southern Hemisphere, the model energy flux is equatorward across 30°S in the Indian, South Pacific, and South Atlantic Oceans. Within the storm track (nominally the band of enhanced wind work between 30°S and 60°S), the energy propagates to the west, in the opposite direction to the weather systems. The westward fluxes in the Southern Ocean have not been previously noted.

### Wind Work on Near-Inertial Motions

Wind work on near-inertial motions is calculated as the vector product of the wind stress and the band-passed surface current ( $\tau \cdot u_I$ ). The spatial distribution of the annual mean wind work closely

follows the storm tracks that run along the northwest margins of the North Pacific and North Atlantic Ocean basins and along the “roaring 40s” (i.e., 40°S) in the southern oceans (gray scale in Figure 2). The global averaged wind work is 0.36 TW (inset in Figure 2), ranging from 0.25 TW in boreal summer (June and July) to 0.40 TW in November, a variation of 60%. Surprisingly, this cycle occurs with roughly the same phase in both hemispheres. The Southern Hemisphere is relatively uniform (variation of 50%, annual mean of 0.22 TW) and is a factor of two stronger than in the Northern Hemisphere in all seasons. The Northern Hemisphere varies from 0.06 to 0.18 TW over the year (variation of 300%). The low-mode signal takes roughly 20 days to propagate from 40°N to the equator, a distance of over 4,000 km ( $2.6 \text{ m s}^{-1}$ , Figure 1D).

### Ratio of Energy Input to Radiation

The average monthly wind work from 30°N to the pole ranges from 35 GW (July) to 150 GW (December). The net southward flux across 30°N ranges

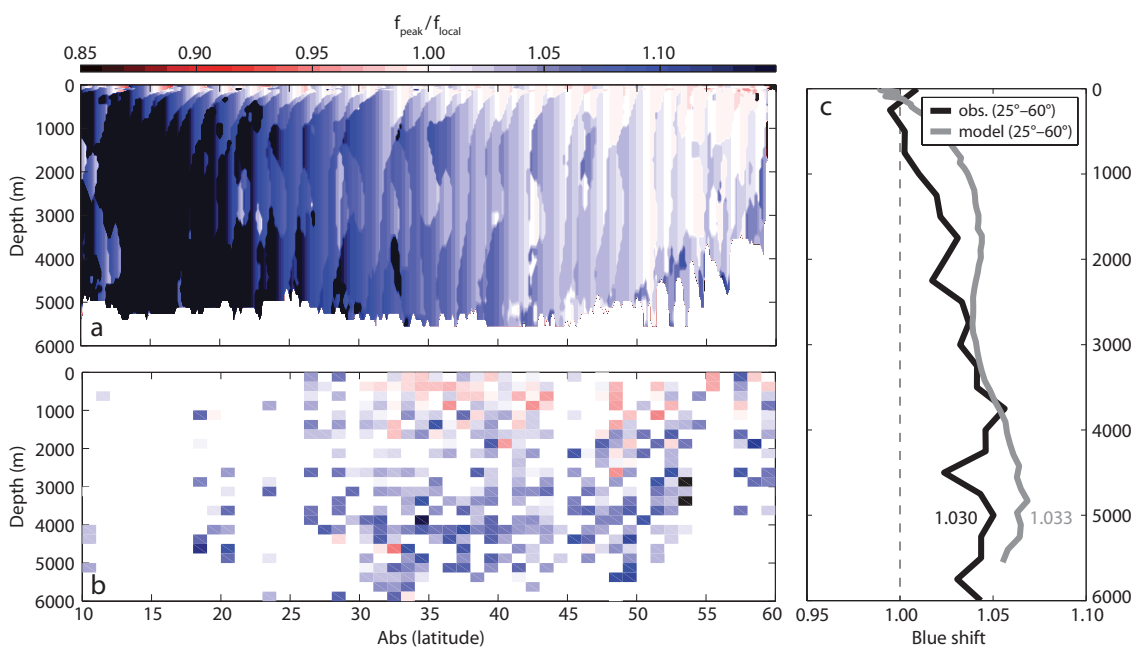


Figure 7. (a) Simulated blue shift as a function of depth and latitude. (b) Blue shift from mooring analysis by Alford (2003a). (c) Profile of modeled and observed blue shift with depth (panels a and b), averaged from 25° to 60° latitude.



from  $1 \text{ kW m}^{-1}$  (July) to  $16 \text{ kW m}^{-1}$  (December). The area integrated energy input south of  $30^\circ\text{S}$  is 150 GW in December (austral summer) and 230 GW in July (austral winter). The equatorward energy flux across  $30^\circ\text{S}$  ranges from 4 GW (December, austral summer) to 20 GW (July, austral winter). Thus, the ratio of the flux leaving the equatorward end of the box to the input ranges from 2% to 16% in the Northern Hemisphere and 2% to 13% in the Southern Hemisphere. The average annual mean ratio for both hemispheres is 7% (see Furiuchi et al., 2008), but an annual average is somewhat misleading because the ratio seems to scale with the wind input and does not represent a response to a specific storm. One possible explanation for the range of values is that wintertime storms work on a deeper mixed layer and thus favor the generation of faster and less-dissipative low modes. It should be stressed that the amount of NIW energy lost from the model in the generation region will be sensitive to the representation of vertical viscous stresses at the base of the mixed layer, to mixed-layer deepening, and to model parameterization of horizontal viscous stresses, so that the absolute ratio of input to output is perhaps uncertain and of less importance to this study than the global patterns of flux.

## SUMMARY AND DISCUSSION

We have presented some aspects of near-inertial wave physics in an eddy-resolving general circulation model (GCM) and made comparisons with moored estimates of peak shift (2,200 estimates at various depths and latitudes), moored estimates of energy flux (80 moorings, mode-1 and -2), and shipboard section(s). The model predicts

that 0.36 TW of energy is transferred to near-inertial motions, which is on the low end of other estimates. This energy input occurs principally under storm tracks and has significant hemispheric and annual variability (Figure 2). The ratio of the spatially integrated wind work over an area to the wave radiation leaving the region is a measure of the amount of wind work that goes into stable, radiating low-mode internal waves, in other words, a measure of the fraction of the energy that dissipates large distances from the storm track. The general pattern is for the waves to radiate equatorward (southeast in the Northern Hemisphere). There is a marked anisotropy between wavenumber  $k$  (east-west) and  $l$  (north-south), with  $l \gg k$ . We find a mode-1 wavelength of about 500–600 km and a mode-3 wavelength of about 200–300 km. The east-west wavelength approaches basin scale. Westward propagation in the Southern Ocean has not been noted previously.

Equatorward fluxes range from 3% to 16% of the energy input. This range of values varies with season and may reflect changes in seasonal mixed-layer depth between July and December. Note that the modeled fluxes are usually about 10–20% weaker than Alford (2003a) and the modeled wind work for the North Pacific is 10–20% higher than Alford (2003a). These two competing differences conspire to reduce the overall estimate of the percent of radiating energy (i.e., their ratio). Note, however, that previous experience with idealized GOLD suggests the simulated ratio can vary by as much as a factor of two, with sensitivity to model resolution and treatment of parameterized viscosity. Future work should examine the role of the mesoscale flows and other factors in determining

this fraction on an event-by-event basis.


Horizontal energy fluxes (Figure 2) agree well with mooring estimates. Looking at depth-latitude sections, energy propagates downward along characteristics (Figure 5). When compared to observed sections, slopes are qualitatively similar, but modeled wavenumbers are substantially lower, and vertical shear is 10 times weaker. Modeled and observed blue shift (Figure 6 and 7) increases from somewhat less than unity at high latitudes and near the surface to 1.3 at depth and near the equator (30% blue shift). This view of the ocean corroborates the Garrett (2001) view, but we find that blue shifting frequently exceeds that predicted by Garrett (2001). The net effect is that the inertial peak becomes increasingly broad and blue shifted equatorward of the storm tracks. We note the absence of reliable observational estimates at latitudes equatorward of  $25^\circ$  precludes any definitive conclusion about blue shift at low latitudes.

The fact that NIW groups can radiate from subpolar latitudes across the equator (Figure 1D) suggests that in the mid-basins (away from western boundary currents), NIW groups are able to pass relatively unscathed through a mesoscale eddy field (Figure 1A). This phenomenon is likely only true for the lower modes. Higher modes have smaller spatial scales and slower phase speeds and are expected to be more sensitive to refraction by mesoscale eddies. We caution that large-scale ocean models are limited in their ability to resolve the high modes, and, therefore, future effort should be directed toward refining our understanding of the radiative versus dissipative partitioning of the energy in near-inertial oceanic motions.

## Consequences for Mixing and Climate

GCMs show sensitivity to the magnitude and vertical and horizontal distribution of mixing (e.g., Simmons et al., 2004b; Jayne, 2009). The global total near-inertial input of 0.36 TW is comparable to the 1 TW of power converted from barotropic to baroclinic tides (Egbert and Ray, 2000), and a substantial fraction of the 2 TW needed to maintain deep ocean stratification (Munk and Wunsch, 1998; Wunsch and Ferrari, 2004). Consequently, inclusion of near-inertial wave supported mixing in GCMs is expected to have an effect on climate simulations (this has already been demonstrated in preliminary simulations by Markus Jochum, National Center for Atmospheric Research, *pers. comm.*, 2012). We caution, however, that in spite of the basic fidelity of slab models for predicting currents, misrepresentation of mixing at the mixed-layer base can lead to uncertainties and biases in the work predicted (Plueddemann and Farrar, 2006). The difference between observed and slab-model work underscores that while we understand the basics of mixed-layer generation, confounding factors such as mixing in transition layers, mesoscale currents, and remotely incident waves may play important roles and, therefore, need to be understood better. Parameterizations of the radiative fraction of internal gravity waves are just beginning to be explored and constitute the authors' contribution to the Internal Waves and Mixing Climate Process Team (CPT; funded by the National Science Foundation, Jennifer MacKinnon, Scripps Institution of Oceanography, PI).

## ACKNOWLEDGMENTS

Harper Simmons was supported by ONR grant N00014-09-1-0399 and NSF (CPT) grant OCE-0968838. Matthew Alford was supported by ONR grant N00014-09-1-0401 and NSF (CPT) grant OCE0968131. Discussions with Eric D'Asaro, Jonathan Nash, and Jennifer MacKinnon, some of which led to a version of Figure 3, are gratefully acknowledged. This work could not have been accomplished without the assistance of Robert Hallberg and Alistair Adcroft of NOAA's Geophysical Fluid Dynamics Laboratory. 

## REFERENCES

- Alford, M.H. 2003a. Improved global maps and 54-year history of wind-work on ocean inertial motions. *Geophysical Research Letters* 30, 1424, <http://dx.doi.org/10.1029/2002GL016614>.
- Alford, M.H. 2003b. Redistribution of energy available for ocean mixing by long-range propagation of internal waves. *Nature* 423:159–162, <http://dx.doi.org/10.1038/nature01628>.
- Alford, M.H. 2010. Sustained, full-water-column observations of internal waves and mixing near Mendocino Escarpment. *Journal of Physical Oceanography* 40:2,643–2,660, <http://dx.doi.org/10.1175/2010JPO4502.1>.
- Alford, M.H., M.F. Cronin, and J.M. Klymak. In press. Annual cycle and depth penetration of wind-generated near-inertial internal waves at Ocean Station Papa in the sub-Arctic Pacific. *Journal of Physical Oceanography*, <http://dx.doi.org/10.1175/JPO-D-11-092.1>.
- Alford, M.H., and M. Whitmont. 2007. Seasonal and spatial variability of near-inertial kinetic energy from historical moored velocity records. *Journal of Physical Oceanography* 37:2,022–2,037, <http://dx.doi.org/10.1175/JPO3106.1>.
- Althaus, A., E. Kunze, and T. Sanford. 2003. Internal tide radiation from Mendocino Escarpment. *Journal of Physical Oceanography* 33:1,510–1,527, [http://dx.doi.org/10.1175/1520-0485\(2003\)033<1510:ITRFME>2.0.CO;2](http://dx.doi.org/10.1175/1520-0485(2003)033<1510:ITRFME>2.0.CO;2).
- Anderson, D., and A. Gill. 1979. Beta dispersion of inertial waves. *Journal of Geophysical Research* 84:1,836–1,842, <http://dx.doi.org/10.1029/JC084iC04p01836>.
- Arbic, B., S. Garner, R. Hallberg, and H. Simmons. 2004. The accuracy of surface elevations in forward near-global barotropic and baroclinic tidal models. *Deep-Sea Research Part II* 51:3,069–3,101, <http://dx.doi.org/10.1016/j.dsr2.2004.09.014>.
- Chaigneau, A., O. Pizarro, and W. Rojas. 2008. Global climatology of near-inertial current characteristics from Lagrangian observations. *Geophysical Research Letters* 35, L13603, <http://dx.doi.org/10.1029/2008GL034060>.
- D'Asaro, E. 1985. The energy flux from the wind into near-inertial motions in the surface mixed layer. *Journal of Physical Oceanography* 15:1,043–1,049, [http://dx.doi.org/10.1175/1520-0485\(1985\)015<1043:TEFTW>2.0.CO;2](http://dx.doi.org/10.1175/1520-0485(1985)015<1043:TEFTW>2.0.CO;2).
- D'Asaro, E. 1989. The decay of wind-forced mixed layer inertial oscillations due to the  $\beta$ -effect. *Journal of Geophysical Research* 94:2,045–2,056, <http://dx.doi.org/10.1029/JC094iC02p02045>.
- D'Asaro, E. 1995. Upper-ocean inertial currents forced by a strong storm. Part I: Data and comparison with linear theory. *Journal of Physical Oceanography* 25:2,909–2,936, [http://dx.doi.org/10.1175/1520-0485\(1995\)025<2909:UOICFB>2.0.CO;2](http://dx.doi.org/10.1175/1520-0485(1995)025<2909:UOICFB>2.0.CO;2).
- D'Asaro, E., and H. Perkins. 1984. A near-inertial internal wave spectrum for the Sargasso Sea in late summer. *Journal of Physical Oceanography* 14:489–505, [http://dx.doi.org/10.1175/1520-0485\(1984\)014<0489:ANIIWS>2.0.CO;2](http://dx.doi.org/10.1175/1520-0485(1984)014<0489:ANIIWS>2.0.CO;2).
- Egbert, G., and R. Ray. 2000. Significant dissipation of tidal energy in the deep ocean inferred from satellite altimeter data. *Nature* 405:775–778, <http://dx.doi.org/10.1038/35015531>.
- Franks, P.J.S. 1995. Thin layers of phytoplankton: A model of formation by near-inertial wave shear. *Deep-Sea Research Part I* 42(1):75–91, [http://dx.doi.org/10.1016/0967-0637\(94\)00028-Q](http://dx.doi.org/10.1016/0967-0637(94)00028-Q).
- Fu, L.L. 1980. Observations and models of inertial waves in the deep ocean. PhD thesis, Massachusetts Institute of Technology.
- Fu, L.L. 1981. Observations and models of inertial waves in the deep ocean. *Reviews of Geophysics and Space Physics* 19:141–170, <http://dx.doi.org/10.1029/RG019i001p00141>.
- Furiuchi, N., T. Hibiya, and Y. Niwa. 2008. Model predicted distribution of wind-induced internal wave energy in the world's oceans. *Journal of Geophysical Research* 113, <http://dx.doi.org/10.1029/2008JC004768>.
- Garrett, C. 2001. What is the “near-inertial” band and why is it different from the rest of the internal wave spectrum? *Journal of Physical Oceanography* 31:962–971, [http://dx.doi.org/10.1175/1520-0485\(2001\)031<0962:WITNIB>2.0.CO;2](http://dx.doi.org/10.1175/1520-0485(2001)031<0962:WITNIB>2.0.CO;2).
- Gill, A.E. 1985. On the behavior of internal waves in the wakes of storms. *Journal of Physical Oceanography* 14:1,129–1,151, [http://dx.doi.org/10.1175/1520-0485\(1984\)014<1129:OTBOIW>2.0.CO;2](http://dx.doi.org/10.1175/1520-0485(1984)014<1129:OTBOIW>2.0.CO;2).

- Griffies, S., A. Biastoch, C. Böning, F. Bryan, G. Danabasoglu, E.P. Chassignet, M.H. England, R. Gerdes, H. Haak, R.W. Hallberg, and others. 2009. Coordinated Ocean-ice Reference Experiments (CORES). *Ocean Modelling* 26:1–46, <http://dx.doi.org/10.1016/j.ocemod.2008.08.007>.
- Hallberg, R. 1997. Stable split time stepping schemes for large-scale ocean modeling. *Journal of Computational Physics* 135:54–65, <http://dx.doi.org/10.1006/jcph.1997.5734>.
- Hallberg, R. 2003. The ability of large-scale ocean models to accept parameterizations of boundary mixing, and a description of a refined bulk mixed-layer model. Internal gravity waves and small-scale turbulence. *Proceedings of the 'Aha Huli' Hawaiian Winter Workshop, University of Hawaii at Manoa, 2003*. P. Müller, ed., Hawaii Institute of Geophysics Special Publication, University of Hawaii.
- Hebert, D., and J.N. Moum. 1994. Decay of a near-inertial wave. *Journal of Physical Oceanography* 24:2,334–2,351, [http://dx.doi.org/10.1175/1520-0485\(1994\)024<2334:DOANIW>2.0.CO;2](http://dx.doi.org/10.1175/1520-0485(1994)024<2334:DOANIW>2.0.CO;2).
- Hosegood, P.J., M.C. Gregg, and M.H. Alford. 2008. Restratification of the surface mixed layer with submesoscale lateral density gradients: Diagnosing the importance of the horizontal dimension. *Journal of Physical Oceanography* 38:2,438–2,460, <http://dx.doi.org/10.1175/2008JPO3843.1>.
- Jackson, L.R., R. Hallberg, and S. Legg. 2008. A parameterization of shear-driven turbulence for ocean climate models. *Journal of Physical Oceanography* 38:519–538, <http://dx.doi.org/10.1175/2007JPO3779.1>.
- Jayne, S.R. 2009. The impact of abyssal mixing parameterizations in an ocean general circulation model. *Journal of Physical Oceanography* 39:1,756–1,775, <http://dx.doi.org/10.1175/2009JPO4085.1>.
- Jiang, J., Y. Lu, and W. Perrie. 2005. Estimating the energy flux from the wind to ocean inertial motions: The sensitivity to surface wind fields. *Geophysical Research Letters* 32, L15610, <http://dx.doi.org/10.1029/2005GL023289>.
- Johnston, T.M.S., and M.A. Merrifield. 2003. Internal tide scattering at seamounts, ridges, and islands. *Journal of Geophysical Research* 108, 3180, <http://dx.doi.org/10.1029/2002JC001528>.
- Komori, N., W. Ohfuchi, B. Taguchi, H. Sasaki, and P. Klein. 2008. Deep ocean inertia-gravity waves simulated in a high-resolution coupled atmosphere ocean GCM. *Geophysical Research Letters* 35, L04610, <http://dx.doi.org/10.1029/2007GL032807>.
- Kunze, E. 1985. Near-inertial wave propagation in geostrophic shear. *Journal of Physical Oceanography* 15:544–565, [http://dx.doi.org/10.1175/1520-0485\(1985\)015<0544:NIWPIG>2.0.CO;2](http://dx.doi.org/10.1175/1520-0485(1985)015<0544:NIWPIG>2.0.CO;2).
- Kunze, E. 1986. The mean and near-inertial velocity fields in a warm-core ring. *Journal of Physical Oceanography* 16:1,444–1,461, [http://dx.doi.org/10.1175/1520-0485\(1986\)016<1444:TMANIV>2.0.CO;2](http://dx.doi.org/10.1175/1520-0485(1986)016<1444:TMANIV>2.0.CO;2).
- Lee, D.-K., and P. Niiler. 1998. The inertial chimney: The near-inertial energy drainage from the ocean surface to the deep layer. *Journal of Geophysical Research* 103(C4):7,579–7,591, <http://dx.doi.org/10.1029/97JC03200>.
- Levine, M.D., and V. Zervakis. 1995. Near-inertial wave propagation into the pycnocline during Ocean Storms: Observations and model comparisons. *Journal of Physical Oceanography* 25:2,890–2,908, [http://dx.doi.org/10.1175/1520-0485\(1995\)025<2890:NIWPIT>2.0.CO;2](http://dx.doi.org/10.1175/1520-0485(1995)025<2890:NIWPIT>2.0.CO;2).
- Lighthill, M.J. 1969. Dynamic response of the Indian Ocean to the onset of the southwest monsoon. *Philosophical Transactions of the Royal Society of London A* 265:45–92, <http://dx.doi.org/10.1098/rsta.1969.0040>.
- Müller, P., and X. Liu. 2000. Scattering of internal waves at finite topography in two dimensions. Part I: Theory and case studies. *Journal of Physical Oceanography* 30:532–549, [http://dx.doi.org/10.1175/1520-0485\(2000\)030<0550:SOIWAF>2.0.CO;2](http://dx.doi.org/10.1175/1520-0485(2000)030<0550:SOIWAF>2.0.CO;2).
- Munk, W.H., and C. Wunsch. 1998. Abyssal recipes II: Energetics of tidal and wind mixing. *Deep-Sea Research Part I* 45:1,977–2,010, [http://dx.doi.org/10.1016/S0967-0637\(98\)00070-3](http://dx.doi.org/10.1016/S0967-0637(98)00070-3).
- Murray, R.J. 1996. Explicit generation of orthogonal grids for ocean models. *Journal of Computational Physics* 126:251–273, <http://dx.doi.org/10.1006/jcph.1996.0136>.
- Plueddemann, A.J., and J.T. Farrar. 2006. Observations and models of the energy flux from the wind to mixed-layer inertial currents. *Deep-Sea Research Part II* 53:5–30, <http://dx.doi.org/10.1016/j.dsr2.2005.10.017>.
- Pollard, R., and R. Millard. 1970. Comparison between observed and simulated wind-generated inertial currents. *Deep-Sea Research* 17:153–175, [http://dx.doi.org/10.1016/0011-7471\(70\)90043-4](http://dx.doi.org/10.1016/0011-7471(70)90043-4).
- Price, J.F., R.A. Weller, and R. Pinkel. 1986. Diurnal cycling: Observations and models of the upper ocean response to diurnal heating, cooling, and wind mixing. *Journal of Geophysical Research* 91(C7):8,411–8,427, <http://dx.doi.org/10.1029/JC091iC07p08411>.
- Rosmond, T., J. Teixeira, M. Peng, T. Hogan, and R. Pauley. 2002. Navy Operational Global Atmospheric Prediction System (NOGAPS): Forcing for ocean models. *Oceanography* 15(1):99–108, <http://dx.doi.org/10.5670/oceanog.2002.40>.
- Silverthorne, K.E., and J.M. Toole. 2006. Seasonal kinetic energy variability of near-inertial motions. *Journal of Physical Oceanography* 39:1,035–1,049, <http://dx.doi.org/10.1175/2008JPO3920.1>.
- Simmons, H.L. 2008. Spectral modification and geographic redistribution of the semi-diurnal tide. *Ocean Modelling* 21:126–138, <http://dx.doi.org/10.1016/j.ocemod.2008.01.002>.
- Simmons, H.L., M.-H. Chang, Y.-T. Chang, S.-Y. Chao, O. Fringer, C. Jackson, and D. Ko. 2011. Modeling and prediction of internal waves in the South China Sea. *Oceanography* 24(4):88–99, <http://dx.doi.org/10.5670/oceanog.2011.97>.
- Simmons, H., R. Hallberg, and B. Arbic. 2004a. Internal-wave generation in a global baroclinic tide model. *Deep-Sea Research Part II* 51:3,043–3,068, <http://dx.doi.org/10.1016/j.dsr2.2004.09.015>.
- Simmons, H.L., L.C. St. Laurent, S.R. Jayne, and A.J. Weaver. 2004b. Tidally driven mixing in a numerical model of the ocean general circulation. *Ocean Modelling* 6:245–263, [http://dx.doi.org/10.1016/S1463-5003\(03\)00011-8](http://dx.doi.org/10.1016/S1463-5003(03)00011-8).
- St. Laurent, L.C., and H.L. Simmons. 2006. Estimates of power consumed by mixing in the ocean interior. *Journal of Climate* 19:4,877–4,890, <http://dx.doi.org/10.1175/JCLI3887.1>.
- Toole, J.M. 2007. Temporal characteristics of abyssal finescale motions above rough bathymetry. *Journal of Physical Oceanography* 37:409–427, <http://dx.doi.org/10.1175/JPO2988.1>.
- Watanabe, M., and T. Hibiya. 2002. Global estimates of the wind-induced energy flux to inertial motions in the surface mixed layer. *Geophysical Research Letters* 29(8), 1239, <http://dx.doi.org/10.1029/2001GL014422>.
- Weller, R.A. 1982. The relation of near-inertial motions observed in the mixed layer during the JASIN (1978) experiment to the local wind stress and to the quasi-geostrophic flow field. *Journal of Physical Oceanography* 12:1,122–1,136, [http://dx.doi.org/10.1175/1520-0485\(1982\)012<1122:TRONIM>2.0.CO;2](http://dx.doi.org/10.1175/1520-0485(1982)012<1122:TRONIM>2.0.CO;2).
- Wunsch, C., and R. Ferrari. 2004. Vertical mixing, energy and the general circulation of the oceans. *Annual Review of Fluid Mechanics* 36:281–314, <http://dx.doi.org/10.1146/annurev.fluid.36.050802.122121>.
- Zhai, X., R.J. Greatbatch, and J. Zhao. 2005. Enhanced vertical propagation of storm-induced near-inertial energy in an eddying ocean channel. *Geophysical Research Letters* 32, L18602, <http://dx.doi.org/10.1029/2005GL023643>.